32nd URSI GASS, Montreal, 19–26 August 2017

Combining self-consistent and test-particle simulations to understand wave-particle interactions between chorus and radiation belt electrons

C. L. da Silva[(1)], R. E. Denton[(1)], M. K. Hudson[(1)], R. M. Millan[(1)]
(1) Department of Physics & Astronomy, Dartmouth College,
6127 Wilder Laboratory, Hanover, NH 03755, USA.

Abstract

In this paper, we present a two-step strategy to quantify wave-particle interactions between chorus and radiation belt electrons. The first step consists of 2-D self-consistent simulations of whistler-mode wave excitation due to electron temperature anisotropy in the inner magnetosphere and its propagation in a meridional plane. The second step consists of test-particle simulations to characterize the interaction between an individual chorus packet and radiation belt electrons. Whistler waves at dawn are excited at the equator and propagate poleward, their wavenormal angle rotates outward and the packets propagate to higher L-shells. Wave interaction with $\sim$100 keV electrons caused concurrent acceleration and increase of pitch-angle. The interaction with $\sim$1 MeV electrons causes pitch-angle scattering into the loss cone in a manner that is not purely explained by a resonant interaction.

1 Introduction

Whistler-mode *chorus* is a discrete (narrowband) emission, typically observed in the inner magnetospheric region coincident with the outer radiation belt (i.e., between $4 \lesssim L \lesssim 7$) [1], and it is typically a dawn-sector phenomena. They are excited by electron cyclotron resonance of energetic electrons (from a few to tens of keVs) injected from the plasmasheet and drifting through that region [2]. Equatorial chorus (located within the magnetic latitude range $|\lambda| < 15°$) is typically observed between midnight and dawn, while higher-latitude chorus ($|\lambda| > 15°$) is mostly observed in the morning sector [1, 3].

Chorus is typically observed between 0.1 and 0.8 Ω_e (where Ω_e corresponds to the equatorial gyrofrequency of electrons), which is roughly equivalent to frequencies between $\sim$100 Hz to 5 kHz in the inner magnetosphere [4]. A salient feature of whistler waves is their dispersive nature, appearing as rising or falling tones in a spectrogram (i.e., $d\omega/dt > 0$ or < 0 where ω is the wave frequency) [5]. But extensive measurements of individual narrowband chorus elements indicate that they not only appear as rising or falling tones, but also as a combination of both (so-called hooks, regular and inverted, and constant tones), or structureless [6].

Whistler-mode chorus has been extensively studied to quantify its role in the population balance of the Earth's radiation belts [2, 7]. Chorus waves can resonantly interact with trapped radiation belt electrons leading to pitch-angle scattering. For MeV electrons in the vicinity of the loss cone, this interaction can lead to electron loss to the atmosphere [8]. Indeed, chorus elements have been correlated both spatially and temporally with microburst-type relativistic electron precipitation [9]. Depending on their energy and pitch-angle, electrons interacting with a chorus element might either gain or lose energy from the wave. Therefore, besides driving pitch-angle scattering losses, chorus waves can locally accelerate electrons to MeV energies, via doppler-shiftted cyclotron resonance [10].

In this paper, we present a two-step strategy to quantify wave-particle interactions between chorus and radiation belt electrons. The first step consists of 2-D self-consistent simulations of whistler-mode wave excitation due to electron temperature anisotropy in the inner magnetosphere. Our hybrid code is designed to capture the generation and propagation of discrete, high-amplitude whistler-mode wave packets, inspired by observations of high amplitude chorus waves [11]. The second step consists of running test-particle simulations to characterize the interaction of individual chorus packets with radiation belt electrons.

2 Model Formulation

Simulation results presented in this paper are obtained using a hybrid fluid/particle-in-cell computer model [12, 13, 14]. The model treats the hot, anisotropic (i.e., ring current) electron population as particles and the background (i.e., the cold, inertialess) electrons as a fluid. Since the hot electrons are only a small fraction of the total population and the cold electrons are assumed to be inertialess, warm (and isotropic) particle electrons are added to the simulation to increase the fraction of particles with mass. We are interested in simulating time intervals up to $\sim 1000\,\Omega_e^{-1}$, which are less than 10% of the proton gyroperiod. Therefore, we can treat ions as a fixed background of positive charge density. The plasma transport equations are coupled to Maxwell's equations and solved in a (2-D) meridional plane. The plasma initial conditions used in the simulation are listed in Table 1.

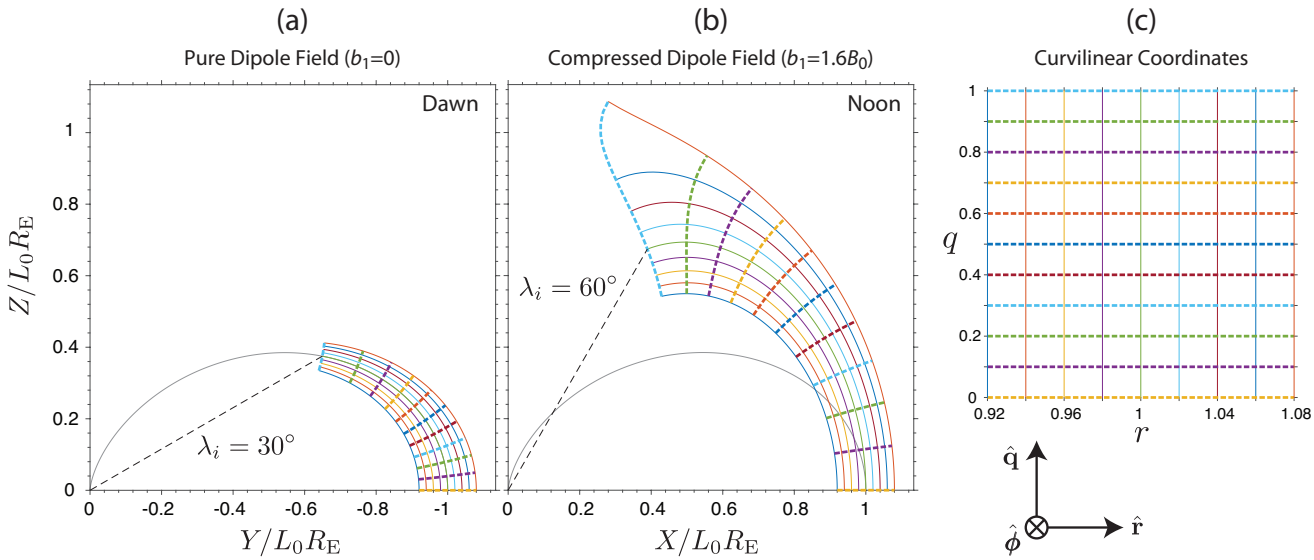

Figure 1. The simulated cartesian meridional plane (Y,Z) at dawn (a) and (X,Z) at noon (b). Panels (a) and (b) are presented in solar magnetic (SM) coordinates (X,Y,Z) normalized to a distance L_0R_E, where L_0 can represent any L-shell of interest (e.g., $L_0 \sim 5.5$ as discussed in the text) and R_E is the Earth radius. Panel (c) shows how the SM coordinates map to the curvilinear coordinates (q,r), with solid and dashed colored lines corresponding to constant r and q values, respectively. Panels (a) and (b) are, respectively, the pure and compressed dipole cases referred to in the manuscript. The grey curve in panels (a) and (b) shows a dipole field line that intercepts the equatorial plane at L_0R_E, just for reference.

Table 1. Simulation Initial Conditions

	Electrons			Positive
Parameters	Hot	Warm	Cold	Ions
Mass (m_e)	1	1	0	∞
Density (cm^{-3})	0.23	0.38	3.19	3.8
$T_\parallel$ (keV)	15	0.01	0	0
$T_\perp/T_\parallel$ (keV)	3	1	1	1

The formation and propagation of whistler-mode chorus waves is heavily determined by the geometry of the background geomagnetic field. Additionally, chorus waves observed at nightside vs. dayside appear to have a significant difference in their latitudinal distribution, as discussed in Section 1. Therefore, it is desirable to design a coordinate system for whistler-mode wave simulation that can follow the topological curvature of the Earth's magnetic field in both the nightside and dayside magnetosphere, i.e., with variable dipolar field curvature from stretched to compressed field lines [15]. For the ease of computational implementation we define our geomagnetic field in a given meridional cross section according to the following analytical expression [16, 15]:

$$\vec{\mathbf{B}} = \hat{\mathbf{R}}\left(-\frac{2B_0}{R^3}+b_1\right)\sin\lambda + \hat{\boldsymbol{\lambda}}\left(\frac{B_0}{R^3}+b_1\right)\cos\lambda\,, \quad (1)$$

where R is the radius normalized to the central L-shell L_0R_E, and λ is the latitude. The only differences between equation (1) and the usual dipole field expression are the terms proportional to the compression factor b_1. By simply tuning the value of b_1, one can construct regular ($b_1 = 0$), compressed ($b_1 > 0$), or stretched ($b_1 < 0$) dipolar field geometries.

Figure 1a shows the simulated region corresponding to the a pure dipolar field geometry representative of the dawn sector. As an illustration we also show in Figure 1b the compressed-dipole configuration that corresponds to local noon (for more details see [14]). Figure 1c shows the corresponding curvilinear coordinate system (q,r,ϕ) used in this paper, where q is a measure of distance along the field lines, r is the L shell (normalized to the central one L_0), and ϕ is the azimuthal angle.

3 Self-Consistent Simulation of Chorus Excitation and Propagation

Figure 2 shows the wave development for the pure dipole background field geometry, that best represents local dawn ($b_1 = 0$). The figure shows the B_ϕ component of the wave magnetic field at three different times, $t\,\Omega_e = 200$, 300, and 400. The figure is shown in the coordinate system of Figure 1c. In Figure 2 we can see the wave development starting at the equator and propagating towards the ionosphere (with a wave vector initially almost parallel to the field lines), which is in agreement with the linear dispersion analysis (see Figure 3 of [14]) and with the typical behavior of midnight-to-dawn chorus as reported by a number of observational investigations [17, 18].

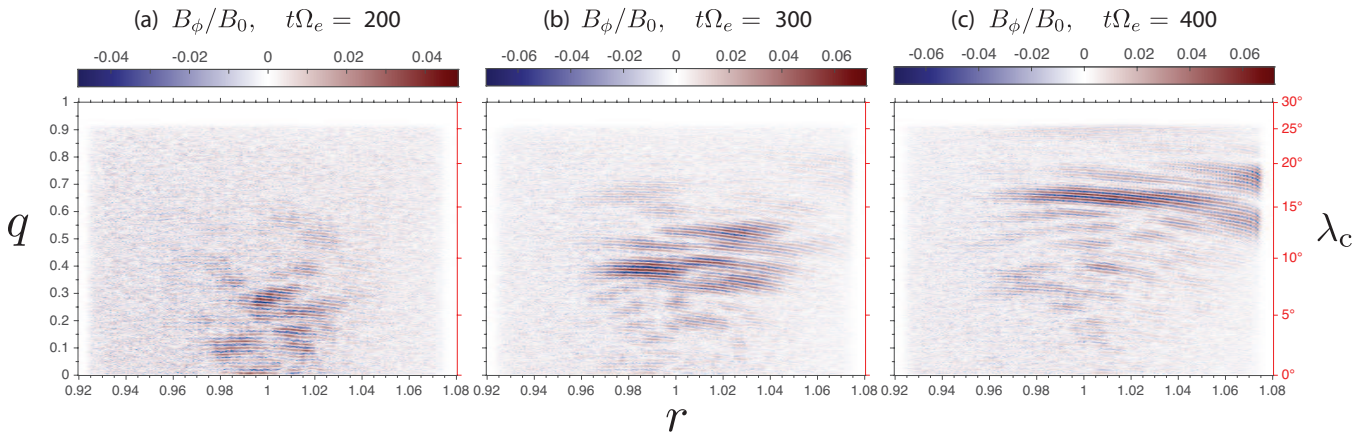

Figure 2. Evolution of out-of-plane magnetic field component B_ϕ. Different panels represent time instants $t\Omega_e = 200$ (a), 300 (b), and 400 (c). The plots are shown in the computational space (q, r). On the right we show the latitude for the central L-shell, λ_c, for reference.

We can also see that the wave packets start to deviate outwards (in the direction of increasing r) as they reach $\sim 5^\circ$ latitude. This effect was previously discussed by [13, 14] and is associated with wave refraction in a plasmatrough-like cold electron density background ($n_{\rm cold}(r) \propto L^{-4}$). The direction of wave energy propagation, with respect to the background magnetic field, is dictated by a balance between the plasma density gradient and magnetic field curvature. The former deflects waves inward, while the latter deflects them outward [19]. A sharper density gradient would produce waves that tend to stay parallel to the field lines, while a smoother gradient (e.g., $n_{\rm cold}(r) = $ constant) would allow waves to refract outward even more. For a comparison between these wave fields at dawn with a simulation at noon, we guide the readers to a previous publication [14].

4 Characterizing Wave-Particle Interactions

We also ran test-particle simulations through the whistler-mode wave fields shown in Figure 2. We selected only the time interval of highest wave power between 200–300 Ω_e^{-1} (i.e., $\Delta t = 100\ \Omega_e^{-1}$). The test particles were two Maxwellian populations of average kinetic energy 100 keV and 1 MeV, the so-called seed and relativistic radiation belt electrons, respectively. We tracked the changes in energy (E) and equatorial pitch-angle ($\alpha_{\rm eq}$) from the beginning to the end of the simulation. Aided of that information, we calculated diffusion coefficients in the format $D_{EE} = \langle \Delta E^2 \rangle / 2\Delta t$ and $D_{\alpha\alpha} = \langle \Delta \alpha_{\rm eq}^2 \rangle / 2\Delta t$. The results are shown in Figure 3.

The curves overlaid in the figure mark the relativistic resonance condition $\omega - k_\parallel v_\parallel = n\Omega_e/\gamma$, where $n = 0, \pm 1, \pm 2, \ldots$. The resonance curves are calculated for a parallel-propagating wave at the equator with a frequency of $\omega = 0.4\,\Omega_e$, which is representative of the waves obtained in our self-consistent simulation (see Figures 3d and 8a of [14]). It can be seen from Figures 3a–3b that the $n = 1$ resonance explains very well the changes in energy and pitch-angle for the 100 keV counterstreaming electrons (with initial $\alpha_{\rm eq} > 90^\circ$). The change in energy and pitch angle happens concurrently indicating a perpendicular acceleration. For the MeV electrons (Figures 3c–3d), the diffusion coefficient maps also seem to follow the resonance curves, with exception of the high diffusion rate at low anti-parallel pitch-angles and high energies. This behavior is shown in the upper-right corner of Figure 3d and it is indicative of nonresonant wave-particle interactions.

Further work is required to fully characterize the resonant and nonresonant wave-particle interactions between whistler-mode chorus and radiation belt electrons.

5 Acknowledgements

This research was supported by NSF AGS-1155934 and NASA grants NNX15AF54G and NNX13AD65G to Dartmouth College. C. L. da Silva thanks the support from the Society of Fellows at Dartmouth College.

References

[1] N. P. Meredith, R. B. Horne, R. M. Thorne, and R. R. Anderson, "Favored regions for chorus-driven electron acceleration to relativistic energies in the Earth's outer radiation belt," *Geophys. Res. Lett.*, vol. 30, no. 16, p. 1871, 2003.

[2] Y. Y. Shprits, D. A. Subbotin, N. P. Meredith, and S. R. Elkington, "Review of modeling of losses and sources of relativistic electrons in the outer radiation belt II: Local acceleration and loss," *J. Atmos. Solar-Terr. Phys.*, vol. 70, no. 14, pp. 1694–1713, 2008.

[3] J.-H. Kim, D.-Y. Lee, J.-H. Cho, D.-K. Shin, K.-C. Kim, W. Li, and T. K. Kim, "A prediction model for the global distribution of whistler chorus wave amplitude developed separately for two latitudinal zones,"

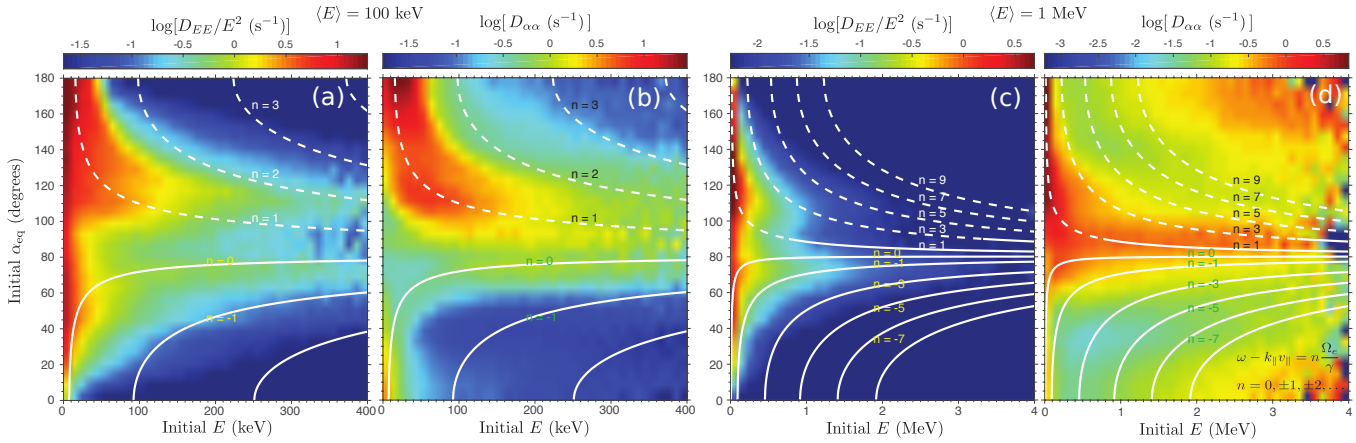

Figure 3. Calculate energy (a,c) and pitch-angle (b,d) diffusion coefficients for relativistic (a,b) and seed (c,d) electron populations. The colormaps show D_{EE} and $D_{\alpha\alpha}$ as function of the initial equatorial pitch-angle (α_{eq}) and energy (E).

J. Geophys. Res., vol. 120, no. 4, pp. 2819–2837, 2015.

[4] H. C. Koons and J. L. Roeder, "A survey of equatorial magnetospheric wave activity between 5 and 8 r_e," *Planet. Space Sci.*, vol. 38, no. 10, pp. 1335–1341, 1990.

[5] R. A. Helliwell, *Whistlers and related ionospheric phenomena*. Stanford, CA: Stanford University Press, 1965.

[6] J. Bortnik and R. Thorne, "The dual role of ELF/VLF chorus waves in the acceleration and precipitation of radiation belt electrons," *J. Atmos. Solar-Terr. Phys.*, vol. 69, no. 3, pp. 378–386, Jan. 2007.

[7] R. M. Thorne, "Radiation belt dynamics: The importance of wave-particle interactions," *Geophys. Res. Lett.*, vol. 37, 2010.

[8] C. F. Kennel and H. E. Petschek, "Limit on stably trapped particle fluxes," *J. Geophys. Res.*, vol. 71, no. 1, pp. 1–28, 1966.

[9] K. R. Lorentzen, J. B. Blake, U. S. Inan, and J. Bortnik, "Observations of relativistic electron microbursts in association with VLF chorus," *J. Geophys. Res.*, vol. 106, no. A4, pp. 6017–6027, 2001.

[10] D. Summers, R. M. Thorne, and F. Xiao, "Relativistic theory of wave-particle resonant diffusion with application to electron acceleration in the magnetosphere," *J. Geophys. Res.*, vol. 103, no. A9, pp. 20 487–20 500, 1998.

[11] C. Cattell, J. R. Wygant, K. Goetz, K. Kersten, P. J. Kellogg, T. von Rosenvinge, S. D. Bale, I. Roth, M. Temerin, M. K. Hudson, R. A. Mewaldt, M. Wiedenbeck, M. Maksimovic, R. Ergun, M. Acuna, and C. T. Russell, "Discovery of very large amplitude whistler-mode waves in Earth's radiation belts," *Geophys. Res. Lett.*, vol. 35, no. 1, Jan. 2008.

[12] Y. Hu and R. E. Denton, "Two-dimensional hybrid code simulation of electromagnetic ion cyclotron waves in a dipole magnetic field," *J. Geophys. Res.*, vol. 114, no. A12, 2009.

[13] S. Wu, R. E. Denton, K. Liu, and M. K. Hudson, "One- and two-dimensional hybrid simulations of whistler mode waves in a dipole field," *J. Geophys. Res.*, vol. 120, no. 3, pp. 1908–1923, 2015.

[14] C. L. da Silva, S. Wu, R. E. Denton, M. K. Hudson, and R. M. Millan, "Hybrid fluid-particle simulation of whistler-mode waves in a compressed dipole magnetic field: Implications for dayside high-latitude chorus," *J. Geophys. Res.*, vol. 121, Dec. 2016.

[15] J. P. McCollough, S. R. Elkington, and D. N. Baker, "The role of Shabansky orbits in compression-related electromagnetic ion cyclotron wave growth," *J. Geophys. Res.*, vol. 117, no. A1, 2012.

[16] K. Kabin, R. Rankin, I. R. Mann, A. W. Degeling, and R. Marchand, "Polarization properties of standing shear Alfven waves in non-axisymmetric background magnetic fields," *Ann. Geophys.*, vol. 25, no. 3, pp. 815–822, 2007.

[17] O. Santolík, D. A. Gurnett, J. S. Pickett, M. Parrot, and N. Cornilleau-Wehrlin, "Spatio-temporal structure of storm-time chorus," *J. Geophys. Res.*, vol. 108, no. A7, Jul. 2003.

[18] W. Li, R. M. Thorne, J. Bortnik, Y. Y. Shprits, Y. Nishimura, V. Angelopoulos, C. Chaston, O. L. Contel, and J. W. Bonnell, "Typical properties of rising and falling tone chorus waves," *Geophys. Res. Lett.*, vol. 38, no. 14, 2011.

[19] U. S. Inan and T. F. Bell, "The plasmapause as a VLF wave guide," *J. Geophys. Res.*, vol. 82, no. 19, pp. 2819–2827, 1977.